Inorganic Chemistry

Article

pubs.acs.org/IC

$BaGe_6$ and $BaGe_{6-x}$: Incommensurately Ordered Vacancies as Electron Traps

Lev Akselrud, Aron Wosylus, Rodrigo Castillo, Umut Aydemir,[†] Yurii Prots, Walter Schnelle, Yuri Grin, and Ulrich Schwarz*

Max-Planck-Institut für Chemische Physik fester Stoffe, Nöthnitzer Straße 40, 01187 Dresden, Germany

Supporting Information

ABSTRACT: We report the high-pressure high-temperature synthesis of the germanium-based framework compounds $BaGe_6$ (P = 15 GPa, T = 1073 K) and $BaGe_{6-x}$ (P = 10 GPa, T = 1073 K) which are metastable at ambient conditions. In $BaGe_{6-x}$, partial fragmentation of the $BaGe_6$ network involves incommensurate modulations of both atomic positions and site occupancy. Bonding analysis in direct space reveals that the defect formation in $BaGe_{6-x}$ is associated with the establishment of free electron pairs around the defects. In accordance with the electron precise composition of $BaGe_{6-x}$ for x = 0.5, physical measurements evidence semiconducting electron transport properties which are combined with low thermal conductivity.

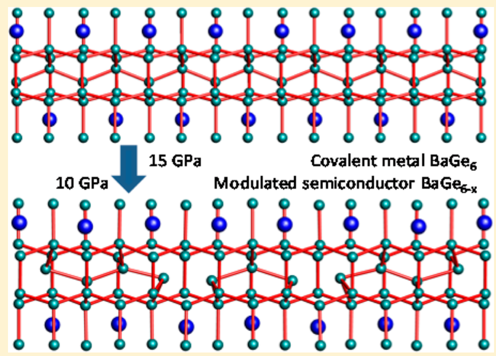

INTRODUCTION

The quest for efficient resource recovery stimulates current interest in basic energy science as a strategic instrument for discovering innovative yet competitive materials. Preparative inorganic chemistry offers access to intermetallic host−guest assemblies as a class of promising compounds which offer beneficial properties like superconductivity[1−4] or thermoelectricity.[5,6] With respect to a rational materials design of covalent frameworks constituted by main group elements, the 8-N rule provides a resilient guideline for the interdependence of chemical composition and network topology.[7] The broad variety of structure motifs and chemical compositions provides prospects for the fine-tuning of electronic structure and charge carrier concentration. We report here on the high-pressure synthesis of two binary compounds, $BaGe_6$ and $BaGe_{6-x}$, with covalently bonded germanium networks.

EXPERIMENTAL SECTION

Synthesis. Preparation and sample handling were realized in argon-filled glove boxes (MBraun, H_2O < 0.1 ppm; O_2 < 0.1 ppm) in order to avoid contamination of the samples. The precursors with a nominal composition of Ba:Ge = 1:5.6 were prepared by arc melting of elemental Ba (Alfa Aesar 99.98%) and Ge (Chempur 99.9999%). The resulting ingots were ground and loaded in crucibles machined from hexagonal boron nitride. High pressures were realized with a Walker-type module employing MgO octahedra of 14 mm edge length.[8] High temperatures were achieved by resistive heating of graphite sleeves. Pressure and temperature calibration had been performed prior to the experiments by in situ monitoring of the resistance changes of bismuth[9] and by performing calibration heating runs with a thermocouple, respectively. Various conditions for temperature and pressure have been applied in the ranges 773(50)−1473(120) K and 10(1.0)−15(1.5) GPa.

A typical experiment included a ramp for compression requiring approximately 3 h. At the maximum pressure, annealing procedures preceded an optional cooling ramp before quenching to room temperature followed by decompression. Single crystals of $BaGe_{6-x}$ are obtained at a pressure of 10(1) GPa using a temperature of 1073(80) K for 10 min before cooling down to 923 K within 10 h. After quenching and pressure release, single crystals can be isolated from the ingot. Metallographic inspection together with WDXS analysis reveal a single phase with composition $Ba_{1.00(1)}Ge_{5.54(8)}$ (see Figure S1 in Supporting Information).

Treatment of $BaGe_{6-x}$ at 15 GPa and 1073 K yields mainly $BaGe_6$ mixed with a new high-pressure form of $BaGe_5$ (Figure S2 in Supporting Information). Upon heating at ambient pressure, $BaGe_{6-x}$ undergoes an irreversible decomposition into α-Ge and the normal-pressure modification of $BaGe_5$ at approximately 689 K (Figures S3 and S4 in Supporting Information).

X-ray Diffraction Data Collection and Processing. Phase identification was performed by powder X-ray diffraction (PXRD) experiments at room temperature. Data collection was realized in transmission mode with a Huber Imaging Plate Guinier camera G670 (Cu $K\alpha_1$ radiation, λ = 1.540 56 Å, 10° ≤ 2θ ≤ 90°, step width 0.005°, 6 × 30 min scans). Unit cell parameters were refined by a least-squares procedure using the WinCSD program package.[10] For measurements with LaB_6 as an internal standard (a = 4.156 92 Å), a STOE-STADIP-MP diffractometer (Bragg−Brentano geometry, Ge-monochromator, Cu $K\alpha_1$ radiation, λ = 1.540 56 Å, 3° ≤ 2θ ≤ 120°, step width 0.02°, 4 × 10 h scans) was used. Single crystal X-ray diffraction data were collected using a Rigaku AFC 7 diffractometer equipped with a Saturn 724 CCD detector (monochromatic Mo $K\alpha$ radiation, λ = 0.710 73 Å). Absorption correction was performed by a multiscan mode. Crystal structure solution and refinement were performed by means of the WinCSD ($BaGe_{6-x}$) and JANA2006 ($BaGe_6$) software

Received: May 28, 2014
Published: November 26, 2014

dx.doi.org/10.1021/ic5021065 | Inorg. Chem. 2014, 53, 12699−12705

Table 1. Crystallographic Data for the Powder X-ray Diffraction Data Refinement of $BaGe_6$

chemical formula	$BaGe_6$
space group	*Cmcm*
T/K	293
a/Å	4.7690(7)
b/Å	10.777(2)
c / Å	12.385(2)
V/Å^3	636.6(2)
formula units, Z	4
radiation, wavelength/Å	Cu Kα1, 1.540 51
diffraction system	Huber G670
measured points, reflns	18 056, 201
measured range, step/deg	$10.025 < 2\theta < 100.300$, 0.005
h(min), k(min), l(min)	0, 0, 0
h(max), k(max), l(max)	4, 10, 12
R(F), R(wP)	0.057, 0.089
GOF	3.45
refined params total, profile	35, 24

Table 2. Atomic Coordinates and Isotropic Displacement Parameters for $BaGe_6$.

atom	Wyckoff position	x/a	y/b	z/c	U_{iso}
Ba	4*c*	0	0.270(2)	$^1/_4$	0.014(5)
Ge1	8*f*	0	0.249(3)	0.536(1)	0.017(3)
Ge2	8*f*	0	0.446(2)	0.644(2)	U_{iso}(Ge1)
Ge3	8*f*	0	0.023(2)	0.598(2)	U_{iso}(Ge1)

packages; estimated standard deviations for the full profile refinements were calculated using an algorithm taking into account local correlations.[10]

Thermal Analysis. Differential scanning calorimetry (DSC) experiments took place in a sealed niobium crucible, using a Netzsch DSC 404C apparatus. Heating and cooling rates of 10 K/min were applied between room temperature and 1273 K.

Energy Dispersive X-ray Analysis. For the metallographic analysis, the samples were polished by using discs of micrometer-sized diamond powders (6, 3, 0.25 μm) in paraffin and investigated with a Philips XL 30 scanning electron microscope (LaB_6 cathode). Energy dispersive X-ray spectroscopy (EDXS) was performed with an attached EDAX Si(Li) detector. The composition of $BaGe_{6-x}$ was determined by wavelength dispersive X-ray spectroscopy (WDXS, Cameca SX 100). For that purpose, Ba_6Ge_{25} and Ge(*cF*8) were used as standards for Ba and Ge, respectively. The WDXS measurements were performed at 10 different spots on the polished surface of a bulk piece (Figure S1 in Supporting Information). Optical microscope images were obtained by a light optical polarization microscope (Zeiss Axioplan 2).

Physical Properties Measurements. Magnetic susceptibility measurements were carried out with a SQUID magnetometer (MPMS XL-7, Quantum Design) on bulk samples of $BaGe_{6-x}$ (x = 0.50; 34.5 mg). External fields between 100 Oe and 70 kOe were applied in the temperature range from 1.8 to 400 K. Electrical resistivity measurements were carried out between 2 and 400 K by a standard ac four-probe technique (PPMS, Quantum Design). For this purpose, a pressed pellet of a polycrystalline sample was prepared with dimensions of $4 \times 2 \times 2$ mm^3 and a mass of approximately 80 mg; because of the uncertainties of the contact geometry, the inaccuracy of the electrical resistivity is estimated to amount to $\pm$20%.

Electronic Structure Calculations. For band structure calculation and bonding analysis of $BaGe_6$ and Ba_7Ge_{39}, the TB-LMTO-ASA program package was used.[11] The Barth–Hedin exchange potential[12] was employed for the LDA calculations. The radial scalar-relativistic Dirac equation was solved to obtain the partial waves. The calculation within the atomic sphere approximation (ASA) includes corrections for the neglect of interstitial regions and partial

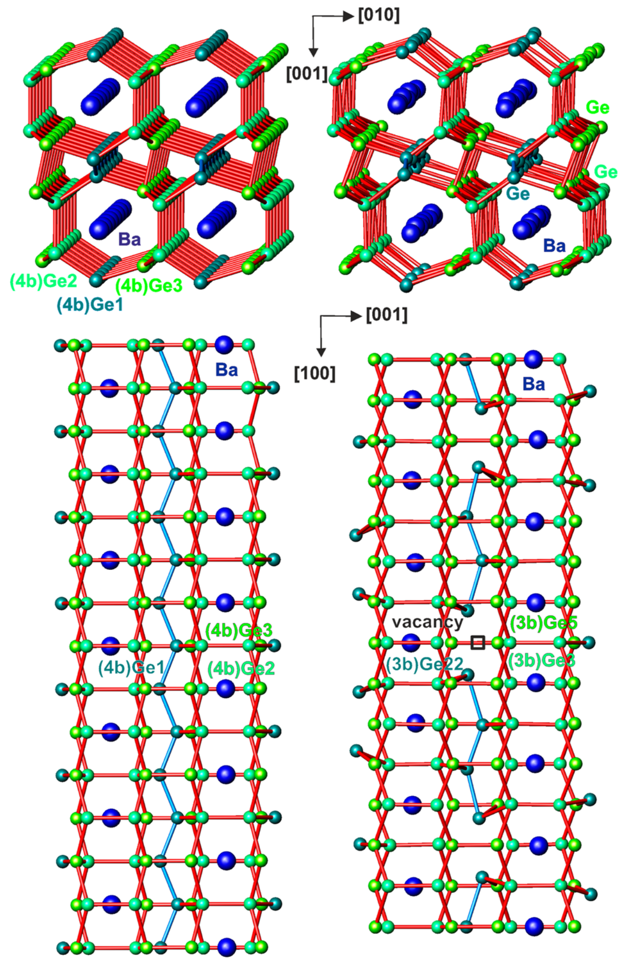

Figure 1. Crystal structures of $BaGe_6$ (left) and the commensurate model of $BaGe_{6-x}$ (Ba_7Ge_{39}, right). The germanium zigzag chain of $BaGe_6$ which is fragmented in $BaGe_{6-x}$ is shown in blue; other short Ge–Ge contacts are indicated in red.

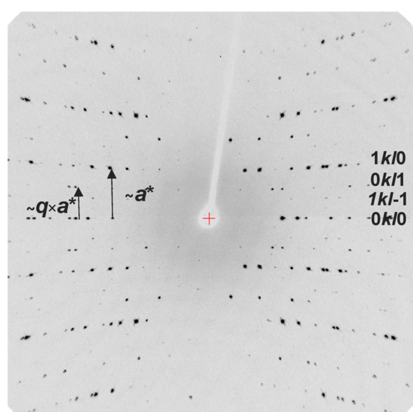

Figure 2. Axial oscillation photo around [100] of $BaGe_{6-x}$. The indexing refers to the structure description in 3 + 1 dimensions. Main reflections are marked as 0*kl*0 and 1*kl*0, respectively; satellite reflections are indicated by 0*kl*1 or 1*kl*−1.

waves of higher order;[13] an addition of empty spheres was not necessary. The following radii of the atomic spheres were applied for the calculations: r(Ba1) = 2.540 Å, r(Ge1) = 1.540 Å, r(Ge2) = 1.539 Å, r(Ge3) = 1.518 Å for $BaGe_6$; r(Ba) = 2.455–2.566 Å, and r(Ge) = 1.480–1.711 Å for Ba_7Ge_{39} (a complete list may be obtained from the corresponding author). Basis sets containing Ba(6s, 5d, 4f) and

Table 3. Experimental Details for the Crystal Structure Determination of $BaGe_{6-x}$

	commensurate model	incommensurate model
chemical formula	$BaGe_{5.57}$ (Ba_7Ge_{39})	$BaGe_{5.5}$
space/superspace group	$Cmc2_1$	$Cmcm(\alpha00)00s$
T/K	293	293
modulation wave vector		$q = 0.5700(1)a^*$
centering	(0, 0, 0), (1/2, 1/2, 0)	(0, 0, 0, 0), (1/2,1/2, 0, 0)
a/Å^a	29.5729(8)	4.2251(2)
b/Å^a	11.2228(3)	11.2208(5)
c/Å^a	12.7992(3)	12.7992(5)
V/Å^3	4247.9(4)	606.79(8)
formula units, Z	28(4)	4
radiation	Mo Kα, 0.710 73	Mo Kα, 0.710 73
diffractometer	Rigaku AFC-7	Rigaku AFC-7
abs correction	multiscan	multiscan
measured reflns	12 063	12 063
unique reflns	4416	2872
$h_{(min)}$, $k_{(min)}$, $l_{(min)}$(, $m_{(min)}$)	−42, −17, −8	0, 0, 0, 0
$h_{(max)}$, $k_{(max)}$, $l_{(max)}$(, $m_{(max)}$)	45, 14, 19	5, 15, 17, 3
refinement	$F \geq 5.9\sigma(F)$	$F \geq 4\sigma(F)$
R(F), R(w) [all], reflns	0.039, 0.041 (1708)	0.034, 0.036 (991)
R(F), R(w) [$hkl0$]		0.025, 0.027 (586)
R(F), R(w) [$hkl1$]		0.063, 0.065 (340)
R(F), R(w) [$hkl2$]		0.070, 0.071 (63)
R(F), R(w) [$hkl3$]		0.057, 0.059 (2)
GOF	1.01	1.01
refined params	217	72
$\Delta\rho_{min}$, $\Delta\rho_{max}$/e Å^3	−2.67, 3.63	−1.26, 1.83

^{a}Cell parameters are refined using powder X-ray diffraction data (Figure S5 and Table S2 in Supporting Information).

Ge(4s, 4p) orbitals were employed for a self-consistent calculation with Ba(6p) and Ge(4d) functions being down-folded. The electron localizability indicator (ELI, ϒ′) was evaluated in the ELI-D representation[14] with the ELI-D module within the program package TB-LMTO-ASA.[11] Topological analysis of the electron density (estimation of the shapes, volumes, and charges of the QTAIM atoms after Bader)[15] and of the electron localizability indicator (distribution of ELI-D and localization of the ELI-D maxima as indicators of the direct covalent atomic interaction) was performed with the program DGrid.[16]

■ RESULTS AND DISCUSSION

Crystal Structures. Refinement of powder X-ray diffraction data (Tables 1 and 2) using full profiles (Figure S2 in Supporting Information) evidence that $BaGe_6$ (Figure 1 left) is isotypic to the binary silicon compounds MSi_6 (M = Ca, Sr, Ba; Eu)[17] and the ternary phase $EuGa_2Ge_4$.[18,19] The atomic arrangement comprises three symmetry-independent four-bonded germanium atoms which form infinite zigzag chains along the [100] direction. These one-dimensional building units are interconnected to a three-dimensional network. The resulting tubular voids house the barium atoms. The shortest Ge−Ge distances from 2.48(4) to 2.63(3) Å within the network are consistent with the values usually observed in Ge-rich intermetallic compounds.[1,3,20] According to the Zintl concept, the electron balance of this connectivity pattern corresponds to $BaGe_6 = [Ba^{2+}][(4b)Ge^0]_6 \times 2e^-$ revealing two excess electrons per formula unit. This is quite a remarkable finding since clathrates with germanium as majority component usually reveal chemical compositions which are charge balanced.

For the germanium-poorer compound $BaGe_{6-x}$, the strongest X-ray diffraction reflections of single crystals indicate an orthorhombic unit cell which is similar to that of $BaGe_6$: b and c of $BaGe_{6-x}$ are larger by 4% and 3%, respectively, while a is 12% shorter. However, long-time X-ray diffraction exposures around the substantially shorter [100] direction reveal a second set of diffraction data with lower intensities (labeled as satellite reflections in Figure 2). In first approximation, the positions of these extra spots are compatible with a 7-fold superstructure along [100].

The solution assuming a commensurate superstructure to the $BaGe_6$ motif succeeds in space group $Cmc2_1$ (Tables 3 and 4). The projection along [010] shows that this atomic arrangement with composition Ba_7Ge_{39} provides characteristic defects at some Ge1 positions of the $BaGe_6$ motif plus displacements of the surrounding framework atoms (Figure 1, right). The majority of the germanium atoms establishes four short contacts, but species at the end of the chain fragments and others surrounding the resulting voids form only three connections. Longer Ge−Ge contacts of these atoms amount to at least 3.017(9) Å and will not be considered here. In comparison to $BaGe_6$, the altered composition and the modified connectivity of the model for $BaGe_{6-x}$ result in a significant reduction of the electron excess according to $[Ba^{2+}]_{7/7}[(3b)Ge^{1-}]_{12/7}[(4b)Ge^0]_{27/7} \times 2/7e^-$.

However, the three-dimensional description of $BaGe_{6-x}$ remains imperfect, e.g., with respect to the large range of displacement parameters resulting for the germanium atoms (Table 4 and Table S1 in Supporting Information). Moreover, the finding that the positions of the superstructure reflections diverge slightly from a commensurate periodicity (see below) is another indication for the inadequacy of the commensurate model.

For advancing to a four-dimensional (3 + 1D) description of the modulation, single-crystal diffraction intensities of the

Table 4. Atomic Coordinates and Equivalent Displacement Parameters for the Commensurate Model of $BaGe_{6-x}$ with composition $BaGe_{5.57}$ (Ba_7Ge_{39})

atom	Wyckoff position	x/a	y/b	z/c	B_{eq} [a]
Ba1	4a	0	0.2858(4)	0.25	1.1(1)
Ba2	8b	0.4295(1)	0.2852(2)	0.2589(5)	1.11(8)
Ba3	8b	0.1416(1)	0.2915(3)	0.2689(4)	0.84(7)
Ba4	8b	0.28665(8)	0.2943(3)	0.2550(6)	0.85(9)
Ge1	4a	0	0.5638(7)	0.3565(7)	0.5(2)
Ge2	4a	0	0.0348(9)	0.9145(8)	1.1(3)
Ge3	4a	0	0.5815(8)	0.1536(8)	0.7(3)
Ge4	4a	0	0.2452(8)	0.9739(7)	0.8(2)
Ge5	4a	0	0.0490(8)	0.6033(8)	1.2(3)
Ge6	8b	0.0723(2)	0.0672(5)	0.3590(6)	0.9(2)
Ge7	8b	0.3551(2)	0.0820(5)	0.3618(6)	0.8(1)
Ge8	8b	0.3548(1)	0.2508(4)	0.0415(5)	0.9(1)
Ge9	8b	0.4283(3)	0.0324(8)	0.9135(7)	1.6(2)
Ge10	8b	0.2135(3)	0.0768(5)	0.3553(6)	1.4(2)
Ge11	8b	0.0714(3)	0.0743(6)	0.1556(6)	0.8(2)
Ge12	8b	0.1434(3)	0.0273(5)	0.6001(6)	1.0(1)
Ge13	8b	0.4275(2)	0.0396(5)	0.6005(6)	0.8(2)
Ge14	8b	0.1428(4)	0.0434(6)	0.9160(6)	1.0(1)
Ge15	8b	0.2859(2)	0.0296(6)	0.9207(6)	0.5(2)
Ge16	8b	0.3568(3)	0.0681(5)	0.1622(5)	0.5(1)
Ge17	8b	0.2147(2)	0.0732(7)	0.1581(7)	1.1(2)
Ge18	8b	0.2859(2)	0.0331(5)	0.6024(6)	0.6(2)
Ge19	8b	0.2772(2)	0.2576(5)	0.9776(6)	1.4(2)
Ge20	8b	0.0865(2)	0.2569(4)	0.0384(6)	1.4(1)
Ge21	8b	0.1902(1)	0.2454(4)	0.0264(5)	1.3(1)
Ge22	8b	0.4435(2)	0.2516(6)	0.9809(6)	1.2(1)

[a] $B_{eq} = 4/3[\ B_{11}(a^*)^2a^2 + ...\ 2B_{23}b^*c^*bc\ \cos(\alpha)]$.

substructure are assigned to indices of the type (*hkl*0), and the weaker superstructure reflections are interpreted as satellites of index (*hklm*) with $m = \pm 0, 1, 2, 3$. The reflections which are classified as observed comply with the additional extinction condition *hk*0*m*: $m = 2n$ yielding the four-dimensional superspace[21] group $Cmcm(\alpha00)00s$ (Table 3).

For a precise determination of lattice parameters and modulation vector, powder X-ray diffraction data are analyzed (Figure S5 and Table S2 in Supporting Information). With a^* being the reciprocal lattice vector of the substructure, the refined modulation vector corresponds to $q = 0.5700(1)a^*$ in comparison to the value of ${}^4/_7a^*$ ($0.5714a^*$) for the identity period of the 7-fold commensurate supercell.

The crystal structure solution of the incommensurate model starts in the three-dimensional space group *Cmcm* using direct methods and the single-crystal X-ray diffraction intensities of the main reflections. Thorough analysis of the resulting $EuGa_2Ge_4$-like atomic pattern[18,19] reveals additional maxima of the difference electron density above and below the Ge1 position in [100] direction (Figure 3). With these features described by introducing the additional germanium position Ge4, the modulation parameters are obtained by least-squares refinements in the superspace group $Cmcm(\alpha00)00s$ using all reflections (including satellites up to 3 order). Refinements proceed by including atomic coordinates and their symmetry-allowed positional modulation amplitudes as well as the atomic displacement parameters in anisotropic approximation. At this stage, the symmetry-allowed occupational modulation amplitudes for the Ge1 and Ge4 position are included. The

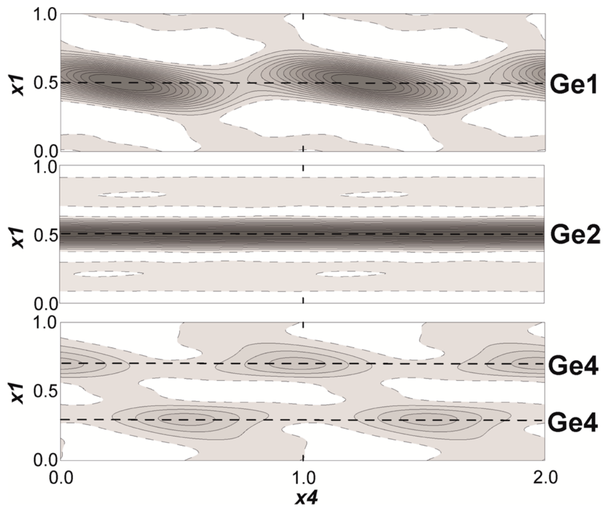

Figure 3. Difference electron density in the *x*1, *x*4 plane of the positions Ge1 and Ge4 (defect occupation, top and bottom, respectively) as well as that of Ge2 (full occupation for comparison, middle) in $BaGe_{6\text{-}x}$. The isolines are drawn with a step size of 25 e/Å^3. The dashed lines indicate the *x*1 positions of the atoms Ge1 ($x = 0.5$, $y = 0.7477$, $z = 0.5363$), Ge2 ($x = 0.5$, $y = 0.07334$, $z = 0.350\ 26$), and Ge4 ($x = 0.5 \pm 0.187$, $y = 0.7557$, $z = 0.5132$), respectively.

calculation range for the occupation modulation amplitudes is obtained from the distribution of the electron density in the (*x*1, *x*4) plane for the Ge1 and Ge4 positions (Figure 3).

For the least-squares refinements of the modulated crystal structure, the Crenel-function technique[22] is applied as implemented in the program package WinCSD.[10] Final refinements include atomic coordinates, their positional modulation amplitudes, atomic displacement parameters, and occupational modulation amplitudes (Tables 5 and 6 as well as Tables S3 and S4 in Supporting Information). The refinement yields a residual value of $R_F = 0.034$, and the resulting interatomic distances (Figure 4) fall into the range from 2.346 to 2.861 Å. The total composition in non-commensurate description corresponds to $BaGe_{6-x}$ with $x = 0.49$, so that the description resembles the electron-precise situation $[Ba^{2+}][(3b)Ge^{1-}]_{4x}[(4b)Ge^0]_{6\text{-}x} \times 0e^-$ ($x = 0.5$) within experimental uncertainty.

Electronic Structure Calculations. The chemical bonding of $BaGe_6$ and $BaGe_{6-x}$ is characterized in direct space by quantum chemical calculations of the electron localizability indicator (ELI).[24] Noninteracting atoms would exhibit spherical symmetry of the ELI distribution while variations, especially in the valence region, are fingerprints of atomic interactions, i.e., covalent bonds or lone pairs. The ELI distribution in $BaGe_6$ reveals that the sixth shell of Ba is basically not visible (Figure 5, top). This finding is attributed to a substantial charge transfer from barium to the electronegative germanium framework. Around the germanium atoms, five ELI-D attractors are observed. Four of these which are located close to the shortest Ge−Ge contacts visualize covalent interactions of the germanium atoms. Beside these four attractors, additional maxima are found for each germanium atom (red in Figure 5, bottom). Such features are absent in the corresponding ELF distribution of the isotypic electron-precise compound $EuGa_2Ge_4$.[19] Thus, these features are assigned to the electron excess of $BaGe_6$.

The ELI-D distribution in Ba_7Ge_{39} (as a commensurate model for $BaGe_{6-x}$) reveals essentially the same charge transfer

dx.doi.org/10.1021/ic5021065 | Inorg. Chem. 2014, 53, 12699−12705

Table 5. Atomic Coordinates, Equivalent Displacement Parameters B_{eq} and Site Occupancy G for $BaGe_{6-x}$ (x = 0.5) in Incommensurate Description

atom	Wyckoff position	x/a	y/b	z/c	B_{eq}	G
Ba	4*c*	0	0.28989(5)	$^1/_4$	1.03(2)	1
Ge1	8*f*	0	0.2476(5)	0.5362(3)	0.80(4)	0.618(4)
Ge2	8*f*	0	0.57333(6)	0.35025(5)	0.81(2)	1
Ge3	8*f*	0	0.03511(6)	0.59242(5)	0.71(4)	1
Ge4	16*h*	0.186(2)	0.2556(7)	0.5131(5)	1.0(3)	0.067(2)

Table 6. Site Occupancy Modulation Parameters for $BaGe_{6-x}$ (x = 0.5) in Incommensurate Description

atom	$\cos(2\pi x_4)$	$\sin(2\pi x_4)$	$\cos(4\pi x_4)$	$\sin(4\pi x_4)$
Ge1[a]			$0.335(7)_p$	$-0.071(5)_p$
Ge4	$0.100(2)_p$	$-0.038(3)_p$	$0.031(3)_p$	$-0.026(2)_p$

[a]Crenel Function: Δ = 0.49, $x4$ = 0.36.

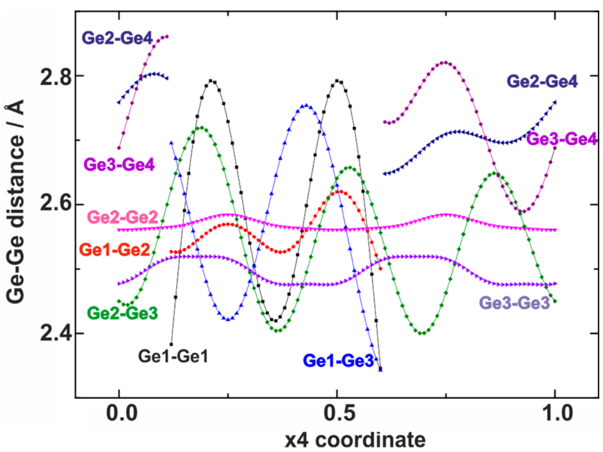

Figure 4. Distances d(Ge−Ge) in $BaGe_{6-x}$ (x = 0.5) as a function of the coordinate $x4$.[23]

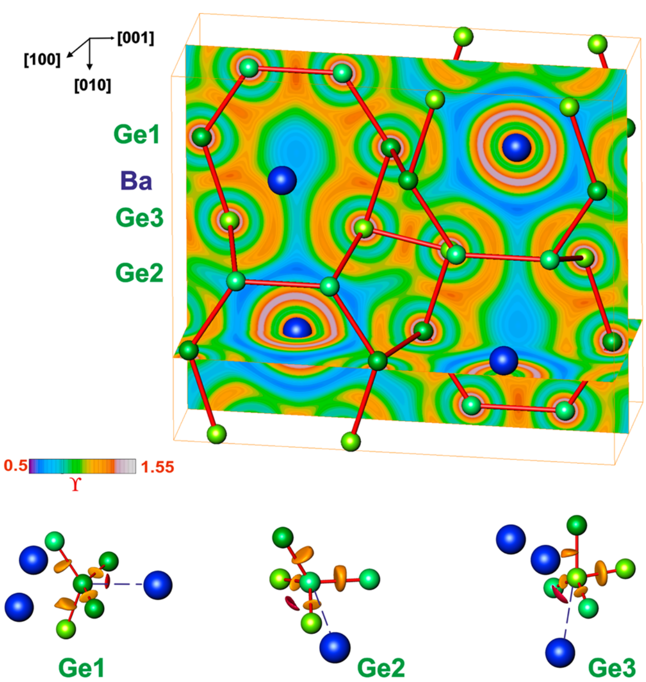

Figure 5. Calculated electron localizability indicator (ELI-D) in $BaGe_6$: (top) distribution in planes perpendicular to the directions [100] and [010]; (bottom) isosurfaces around the germanium atoms.

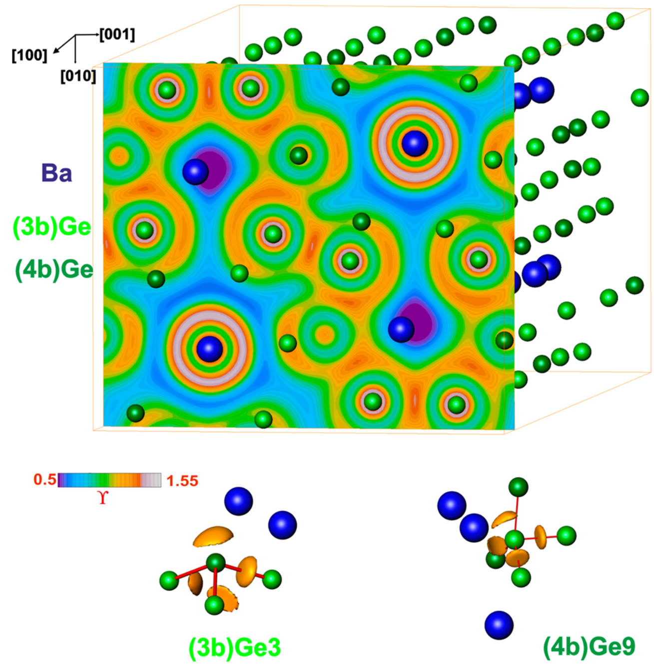

Figure 6. Electron localizability indicator (ELI-D) in Ba_7Ge_{39} as a commensurate model for $BaGe_{6-x}$: (top) distribution in the plane perpendicular to [100]; (bottom) isosurfaces around a selected three-bonded (left) and four-bonded (right) germanium atom, respectively. The numbering of the germanium atoms refers to that of Table 4.

from barium to the germanium framework as in $BaGe_6$ (Figure 6, top). Only four ELI-D attractors are observed around each germanium atom (Figure 6, bottom). Most of these are located close to Ge−Ge contacts visualizing two-center bonds. However, some of the attractors are monosynaptic; i.e., their basins contact only the core basin of one germanium atom, thus visualizing three-bonded germanium atoms with lone-pair-like features.

The electronic density of states (DOS) for $BaGe_6$ reveals a high density of states at the Fermi level and a rudimentary pseudogap at $E \approx -0.6$ eV (Figure 7, top). The top of the valence band is mainly formed by Ge(p) states, and more than half of these are contributed by Ge1, implying the important role of these atoms in the electrical conductivity of the compound.

The formation of defects in $BaGe_{6-x}$ (Ba_7Ge_{39}) does not only shift the Fermi level to lower energies, but opens also a pronounced pseudogap by reducing the DOS around the Fermi level by a factor of 3 in comparison to $BaGe_6$ (Figure 7, bottom). These changes close to E_F are in full accord with a substantial reduction of the electron excess by the vacancy formation.

Physical Properties. In agreement with the observed systematics of the electronic density of states, the high-field magnetic susceptibility $\chi(T) = M/H$ of $BaGe_{6-x}$ (Figure S6 in Supporting Information) is negative indicating diamagnetic

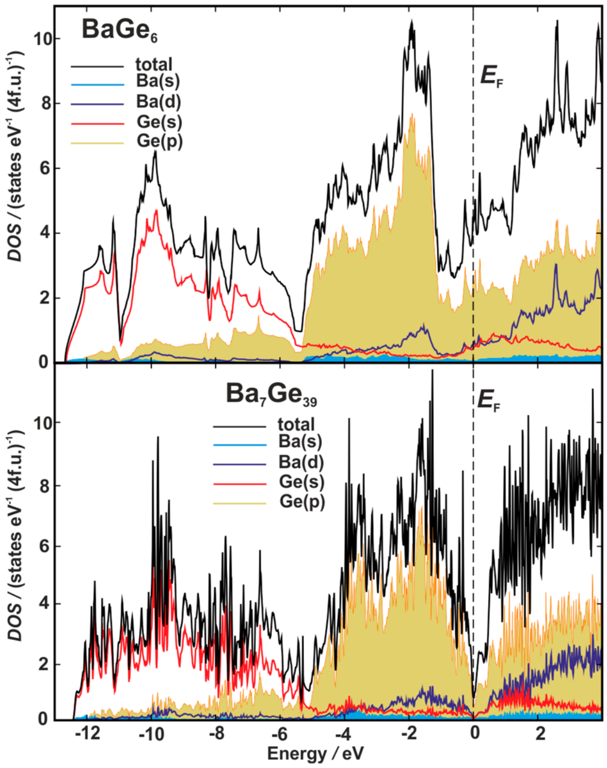

Figure 7. Electronic density of states for $BaGe_6$ (top) and the commensurate structure model of $BaGe_{6-x}$ ($Ba_7Ge_{39,}$ bottom). The DOS of $BaGe_{6-x}$ is scaled to one Ba atom as in $BaGe_6$; i.e., one formula unit of Ba_7Ge_{39} is renormalized to $Ba_{7/7}Ge_{39/7}$ or $BaGe_{5.57}$.

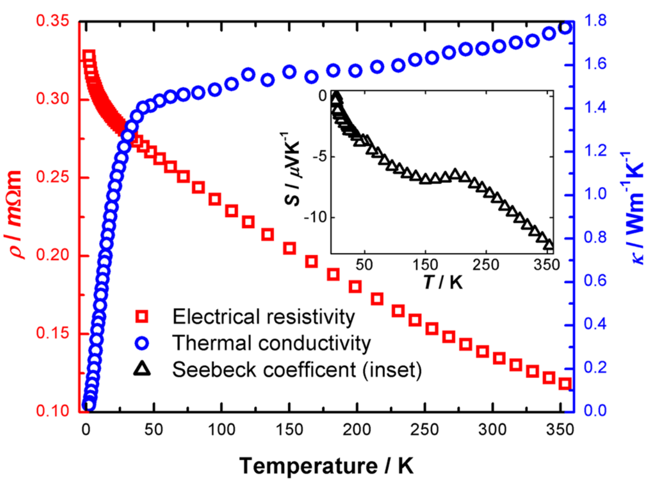

Figure 8. Electronic and thermal transport properties of $BaGe_{6-x}$ at temperatures between 2 and 353 K.

behavior. The value χ_0 of $-120(10) \times 10^{-6}$ emu mol^{-1} at $T = 0$ is in fair agreement with the sum of the diamagnetic increments[25,26] which results in -90×10^{-6} emu mol^{-1} for $BaGe_{6-x}$ ($x = 0.5$). These results evidence diamagnetic and, thus, semiconducting behavior of the Ge-deficient sample. Consistently, the electrical resistivity ρ(T) decreases slightly and almost linearly with temperature indicating a semiconducting characteristic. The high absolute values indicate a strongly doped (defects, impurities) semiconductor with the result that also the Seebeck coefficient $S_{300\ K}$ is reduced to a value of 10 μVK^{-1} which would be more typical for a metallic conductor. The thermal conductivity κ(T) of the modulated framework ensemble ($\kappa_{300\ K} = 1.7$ W m^{-1} K^{-1}) is low (Figure 8) and of the typical order found in cage compounds, e.g., clathrates like $Ba_8Ni_{3.5}Ge_{42.1}\square_{0.4}$ (□ represents a vacancy).[27] The resulting thermoelectric figure of merit, $ZT = S^2 \times T/(\kappa \times \rho)$, remains small because the effects caused by the high charge-carrier concentration clearly overcompensate for the beneficial contribution of the low thermal conductivity.

■ CONCLUSION

The crystal structures of $BaGe_6$ and $BaGe_{6-x}$ ($x = 0.5$) exhibit a clear interdependence of network topology and electron balance. $BaGe_6$ features four-bonded framework atoms and a surplus of electrons, a situation more frequently observed for silicon-rich compounds.[17] In $BaGe_{6-x}$, those germanium atoms which engird the defects are three-bonded. The simultaneous localization of excess electrons in lone pairs provides efficient electron traps and, thus, an effective decoupling of electrical and thermal conductivity. Although similar phenomena have already been observed in phases like the structurally related $SrGe_{5.5}\square_{0.5}$[28] or type-I clathrates like $K_8Ge_{44}\square_2$,[7] the arrangement of defects normally preserves conventional three-dimensional symmetry. The unique feature of $BaGe_{6-x}$ is that the requirements for an electron-precise phase according to the 8-N rule and the Zintl concept are fulfilled by the formation of lattice defects exhibiting incommensurate modulations.

■ ASSOCIATED CONTENT

Supporting Information

Metallography and additional crystallographic information for $BaGe_{6-x}$; thermal analysis data and magnetic measurements for $BaGe_{6-x}$. This material is available free of charge via the Internet at http://pubs.acs.org.

■ AUTHOR INFORMATION

Corresponding Author

*E-mail: schwarz@cpfs.mpg.de.

Present Address

†California Institute of Technology, Pasadena, California 91125, United States.

Author Contributions

The manuscript was written through contributions of all authors. All authors have given approval to the final version of the manuscript.

Funding

R.C. gratefully acknowledges the Becas Chile program for a doctoral grant.

Notes

The authors declare no competing financial interest.

■ ACKNOWLEDGMENTS

We thank Susann Leipe for high-pressure syntheses, Christina Drathen (ID31 at the ESRF, Grenoble) for supporting synchrotron X-ray powder diffraction experiments, Marcus Schmidt and Susann Scharsach for DTA characterization, Ulrich Burkhardt, Monika Eckert, and Sylvia Kostmann for metallographic investigations, as well as Ralf Koban for physical measurements.

■ REFERENCES

(1) (a) Fukuoka, H.; Yamanaka, S. *Phys. Rev. B* **2003**, *67*, 094501. (b) Meier, K.; Cardoso-Gil, R.; Schnelle, W.; Rosner, H.; Burkhardt, U.; Schwarz, U. *Z. Anorg. Allg. Chem.* **2010**, *636*, 1466–1473.

(2) (a) Yamanaka, S.; Enishi, E.; Fukuoka, H.; Yasukawa, M. *Inorg. Chem.* **2000**, *39*, 56−58. (b) Fukuoka, H.; Kiyoto, J.; Yamanaka, S. *Inorg. Chem.* **2003**, *42*, 2933−2937. (c) Rachi, T.; Yoshino, H.; Kumashiro, R.; Kitajima, M.; Kobayashi, K.; Yokogawa, K.; Murata, K.; Kimura, N.; Aoki, H.; Fukuoka, H.; Yamanaka, S.; Shimotani, H.; Takenobu, T.; Iwasa, Y.; Sasaki, T.; Kobayashi, N.; Miyazaki, Y.; Saito, K.; Guo, F. Z.; Kobayashi, K.; Osaka, K.; Kato, K.; Takata, M.; Tanigaki, K. *Phys. Rev. B* **2005**, *72*, 144504. (d) San Miguel, A.; Toulemonde, P. *High Pressure Res.* **2005**, *25*, 159−185. (e) Toulemonde, P.; San Miguel, A.; Merlen, A.; Viennois, R.; Le Floch, S.; Adessi, Ch.; Blase, X.; Tholence, J. L. *J. Phys. Chem. Solids* **2006**, *67*, 1117−1121. (f) Tang, J.; Xu, J.; Heguri, S.; Fukuoka, H.; Yamanaka, S.; Akai, K.; Tanigaki, K. *Phys. Rev. Lett.* **2010**, *105*, 176402.

(3) Schnelle, W.; Ormeci, A.; Wosylus, A.; Meier, K.; Grin, Yu.; Schwarz, U. *Inorg. Chem.* **2012**, *51*, 5509−5511.

(4) Schwarz, U.; Wosylus, A.; Rosner, H.; Schnelle, W.; Ormeci, A.; Meier, K.; Baranov, A.; Nicklas, M.; Leipe, S.; Müller, C. J.; Grin, Yu. *J. Am. Chem. Soc.* **2012**, *134*, 13558−13561.

(5) (a) Prokofiev, A.; Sidorenko, A.; Hradil, K.; Ikeda, M.; Svagera, R.; Waas, M.; Winkler, H.; Neumaier, K.; Paschen, S. *Nat. Mater.* **2013**, *12*, 1096−1101. (b) Bentien, A.; Pacheco, V.; Paschen, S.; Grin, Y.; Steglich, F. *Phys. Rev. B* **2005**, *71*, 165206. (c) Pacheco, V.; Bentien, A.; Carrillo-Cabrera, W.; Paschen, S.; Steglich, F.; Grin, Yu. *Phys. Rev. B* **2005**, *71*, 165205. (d) Saramat, A.; Svensson, G.; Palmqvist, A. E. C.; Stiewe, C.; Mueller, E.; Platzek, D.; Williams, S. G. K.; Rowe, D. M.; Bryan, J. D.; Stucky, G. D. *J. Appl. Phys.* **2006**, *99*, 023708. (e) Toberer, E. S.; Christensen, M.; Iversen, B. B.; Snyder, G. J. *Phys. Rev. B* **2008**, *77*, 075203. (f) Zhang, H.; Borrmann, H.; Oeschler, N.; Candolfi, C.; Schnelle, W.; Schmidt, M.; Burkhardt, U.; Baitinger, M.; Zhao, J.-T.; Grin, Yu. *Inorg. Chem.* **2011**, *50*, 1250−1257.

(6) (a) Nolas, G. S.; Cohn, J. L.; Slack, G. A.; Schujman, S. B. *Appl. Phys. Lett.* **1998**, *73*, 178−180. (b) Nolas, G. S.; Poon, J.; Kanatzidis, M. *MRS Bull.* **2006**, *31*, 199−205. (c) Nolas, G. S.; Slack, G. A.; Schujman, S. B. *Semiconductors and Semimetals*; Academic Press: San Diego, CA, 2000; Vol. *69*.

(7) Baitinger, M.; Böhme, B.; Ormeci, A.; Grin, Yu. Solid State Chemistry of Clathrate Phases: Crystal Structure, Chemical Bonding and Preparation Routes. In *Clathrates*; Nolas, G. S., Ed.; Springer: New York, 2014.

(8) Walker, D.; Carpenter, M. A.; Hitch, C. M. *Am. Mineral.* **1990**, *75*, 1020−1028.

(9) Young, D. A. *Phase Diagrams of the Elements*; UC Press: Oakland, CA, 1991; p 122 and references therein.

(10) (a) Akselrud, L.; Grin, Yu. *J. Appl. Cystallogr.* **2014**, *47*, 803−805. (b) Petricek, V.; Dusek, M.; Palatinus, L. *Jana2006. Structure Determination Software Programs*; Institute of Physics: Praha, Czech Republic, 2006. (c) Petricek, V.; Dusek, M.; Palatinus, L. *Z. Kristallogr.* **2014**, *229*, 345. (d) Berar, J.-F.; Lelann, P. *J. Appl. Crystallogr.* **1991**, *24*, 1−5.

(11) Jepsen, O.; Burkhardt, A.; Andersen, O. K. *The Program TB-LMTO-ASA, Version 4.7*; Max-Planck-Institut für Festkörperforschung: Stuttgart, 1999.

(12) von Barth, U.; Hedin, L. *J. Phys. C* **1972**, *5*, 1629−1642.

(13) Andersen, O. K. *Phys. Rev. B* **1975**, *12*, 3060−3083.

(14) (a) Kohout, M. *Int. J. Quantum Chem.* **2004**, *97*, 651−658. (b) Kohout, M.; Wagner, F. R.; Grin, Yu. *Int. J. Quantum Chem.* **2006**, *106*, 1499−1507. (c) Kohout, M. *Faraday Discuss.* **2007**, *135*, 43−54.

(15) Bader, R. F. W. *Atoms in Molecules, A Quantum Theory*; Clarendon Press and Oxford University Press Inc.: New York, 1994.

(16) Kohout, M. *DGrid, version 4.6*; Radebeul, 2010.

(17) (a) Yamanaka, S.; Maekawa, S. *Z. Naturforsch.* **2006**, *B61*, 1493−1499. (b) Wosylus, A.; Prots, Yu.; Burkhardt, U.; Schnelle, W.; Schwarz, U.; Grin, Yu. *Z. Naturforsch.* **2006**, *B 61*, 1485−1492. (c) Wosylus, A.; Prots, Yu.; Burkhardt, U.; Schnelle, W.; Schwarz, U.; Grin, Yu. *Solid State Sci.* **2006**, *8*, 773−781. (d) Wosylus, A.; Prots, Yu.; Burkhardt, U.; Schnelle, W.; Schwarz, U. *Sci. Technol. Adv. Mater.* **2007**, *8*, 383−388.

(18) Bryan, J. D.; Stucky, G. D. *Chem. Mater.* **2001**, *13*, 253−257.

(19) Carrillo-Cabrera, W.; Paschen, S.; Grin, Yu. *J. Alloys Compd.* **2002**, *333*, 4−12.

(20) (a) Fukuoka, H.; Baba, K.; Yoshikawa, M.; Ohtsu, F.; Yamanaka, S. *J. Solid State Chem.* **2009**, *182*, 2024−2029. (b) Meier, K.; Koz, C.; Kerkau, A.; Schwarz, U. *Z. Kristallogr.—New Cryst. Struct.* **2009**, *224*, 349−350. (c) Meier, K.; Kerkau, A.; Schwarz, U. *Z. Kristallogr.—New Cryst. Struct.* **2009**, *224*, 373−374. (d) Fukuoka, H.; Yoshikawa, M.; Baba, K.; Yamanaka, S. *Bull. Chem. Soc. Jpn.* **2010**, *83*, 323−327. (e) Fukuoka, H.; Tomomitsu, Y.; Inumaru, K. *Inorg. Chem.* **2011**, *50*, 6372−6377. (f) Fukuoka, H.; Suekuni, K.; Onimaru, T.; Inumaru, K. *Inorg. Chem.* **2011**, *50*, 3901−3906. (g) Meier, K.; Wosylus, A.; Cardoso-Gil, R.; Burkhardt, U.; Curfs, C.; Hanfland, M.; Grin, Yu.; Schwarz, U. *Z. Anorg. Allg. Chem.* **2012**, *638*, 1446−1451.

(21) Janssen, T.; Janner, A.; Looijenga-Vos, A.; de Wolff, P. M. Incommensurate and Commensurate Modulated Structures. In *International Tables for Crystallography*, 3rd ed.; Prince, E., Ed.; Kluwer Academic Publisher: Dordrecht, 2004; Vol. C, Chapter 9.8, pp 907−955.

(22) Petrícek, V.; van der Lee, A.; Evain, M. *Acta Crystallogr., Sect. A* **1995**, *51*, 529−535.

(23) The distances are plotted against the $x4$ coordinate with the following starting positions of the atoms: Ge1 (0, 0.2476, 0.5363), Ge1 ($^1/_2$, 0.2524, 0.4637), Ge2 (0, 0.4267, 0.6497), Ge3 (0, 0.0351, 0.5924); Ge2 (0, 0.5734, 0.3503), Ge2 (0, 0.5734, 0.1497), Ge3 (1/2, 0.4649, 0.4076), Ge4 (0.1869, 0.7443, 0.4868); Ge3 (0, 0.0351, 0.5924), Ge3 (0, −0.0351, 0.4076), Ge4 (0.1869, 0.2557, 0.5132).

(24) (a) Butovskii, M. V.; Döring, Ch.; Bezugly, V.; Wagner, F. R.; Grin, Yu.; Kempe, Rh. *Nat. Chem.* **2010**, *2*, 741−744. (b) Wagner, F. R.; Kohout, M.; Grin, Yu. *J. Phys. Chem. A* **2008**, *112*, 9814−9828. (c) Wagner, F. R.; Bezugly, V.; Kohout, M.; Grin, Yu. *Chem.—Eur. J.* **2007**, *13*, 5724−5741.

(25) Selwood, P. W. *Magnetochemistry*; Interscience: New York, 1956.

(26) Landoldt-Börnstein. *Numerical Data and Functional Relationships in Science and Technology, New Series, II/16, Diamagnetic Susceptibility*; Springer: Heidelberg, 1986.

(27) Nguyen, L. T. K.; Aydemir, U.; Baitinger, M.; Bauer, E.; Borrmann, H.; Burkhardt, U.; Custers, J.; Haghighirad, A.; Höfler, R.; Luther, K. D.; Ritter, F.; Assmus, W.; Grin, Yu.; Paschen, S. *Dalton Trans.* **2010**, *39*, 1071−1077.

(28) Fukuoka, H.; Yamanaka, S.; Matsuoka, E.; Takabatake, T. *Inorg. Chem.* **2005**, *44*, 1460−1465.